The Day After: Post-Collision Distribution of Remnants, Fragments and Debris Clouds in the Outer Solar System

Gal Sarid & Jennifer Larson, Florida Space Institute & Department of Physics, University of Central Florida, Orlando, FL, USA.
gal.sarid@ucf.edu

Introduction

Icy-rocky bodies beyond the orbit of Jupiter preserve crucial information about the formation and evolution of the outer planetary disk. The parent-body dwarf planets formed and evolved within a large population of planetesimals, ranging in size from 10s to a few 1000s of km in diameter, prior to and during the planet formation epoch [1, 2]. There is increasing evidence that there is a variety of systems that exist in complex physical states (multiple satellites, potential rings, conjectured families), which probably formed and evolved early, largely through erosive or disruptive collisions between at least partially differentiated bodies.

Collisions that deform and disrupt both target and projectile bodies change the configuration of the original system. It produces remnant bodies that may differ in composition, angular momentum and orbit. These can span a large size range, from the target body itself, to smaller satellites, to ejected fragments, even down to unbound clouds of debris [3, 4]. The variety of outcomes from erosive collisions has been invoked to explain several outstanding issues in the solar system (Moon formation, Mercury's origin, Pluto's multiple moons, Haumea's collisional family) [5, 6, 7, 8, 9, 10].

We are interested in understanding the fate of the released material as relating to its orbital and compositional distribution. This can be either bound material, as disks or satellites, or unbound fragments and debris clouds. Remnant material, which has velocities greater than the mutual escape velocity of the target-bound system and has not been accreted rapidly after the collision event, may experience short and long-term dynamical perturbations and evolve on diverging orbits. We present here examples of both bound material and unbound material, as dependent on the initial conditions of the collision system (target and projectile bodies).

Collision Systems

The internal temperature profile and differentiation state of our presumed colliding bodies are taken from a large suite of previously calculated thermal evolution models for mid-sized and large icy bodies (assuming water ice and chondritic composition for the rock component) [e.g., 11, 12]. We have conducted 3D numerical simulations of collisions between such bodies with a modified version of the *GADGET2* code.

GADGET2 is a code for N-body/SPH simulations [13], which has been modified to handle tabulated equations of state [14]. It is fully conservative in integrating hydrodynamic equations [15], maintaining energy and entropy conservation even when smoothing lengths vary adaptively [16]. In our scheme planetary bodies are represented by a spherically symmetric overlapping particles whose individual response to the governing equations are tracked as a function of time. Each particle represents a fixed mass of a given composition, and its spatial extent varies throughout (specified by a density kernel and a smoothing length). Without prescribed material strength, it strictly represents collisions only in the gravity regime. This version has been used in several studies of planetary collisions, including both rocky and icy materials, to examine the outcomes of oblique collisions [5, 10, 11, 12, 14, 17].

Our simulations have covered a range in target and projectile sizes and mass ratios, impact velocities (~1-7 times the mutual escape velocity) and impact angles, corresponding to events of head-on collisions to barely grazing encounters. **Table 1** summarizes these parameters. **Figure 1** shows an example of an erosive and partial accretion event between 2 differentiated bodies, resulting in some unbound ejecta and bound fragments.

Table 1: Parameters for collision simulations of differentiated icy bodies:

Radius [km]	**150 – 1200**
Impact velocity [km/s]	**0.5 – 5**
Impact angle [deg]	**0 – 60**
Initial density (g/cm^3)	**0.97 – 2.00**
Rock-Ice ratio	**0.1 – 10**
Eq. of state	**Water (Stewart 5 -phase), serpentine and silica (ANEOS)**
# of SPH particles	**25,000 – 100,000**

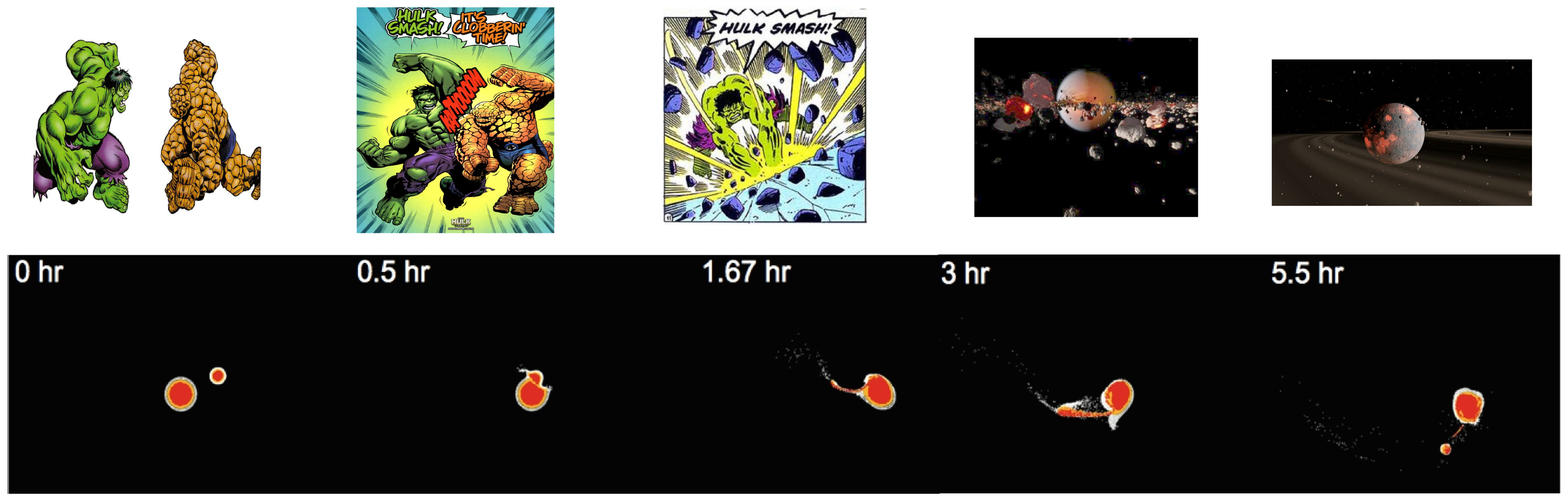

Figure 1: Snapshots of collision between 2 differentiated icy bodies, with a crust (water ice, white), mantle (serpentine, orange) and core (silica, red). Target/projectile mass ratio = 8, rock/Ice ratio = 2.5, impact velocity = 1 km/s, impact angle = 45 deg.
There are several smaller fragments being ejected that are predominantly icy or rocky. End distribution of material close to and on the surface is much less homogeneous than initially, with larger fractions of rock. Secondary remnant's composition also differs significantly from initial state.

Top row is an artistic depiction of the process, for the reader's amusement.

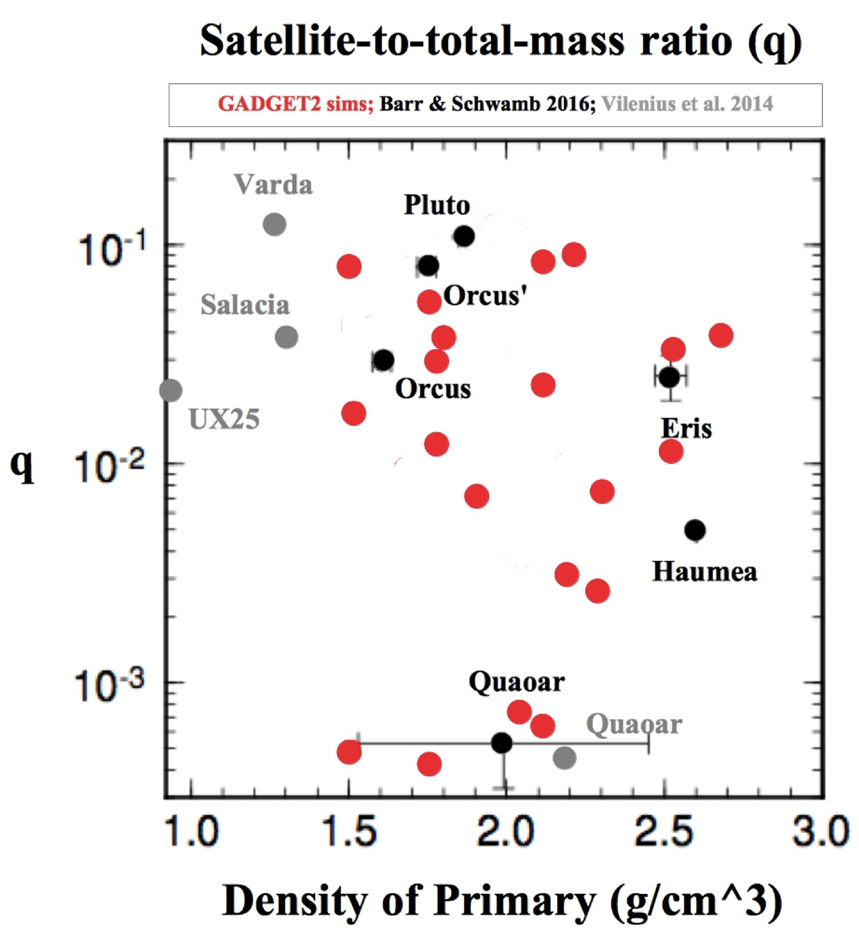

Representation of the largest trans-Neptunian objects (from Wikimedia Commons).

All have moons.

Figure 2: Satellite-to-total mass ratio, as a function of the primary body density.Black and gray circles are measured values and errors several TNOs, reproduced from [20, 21] and references therein. Red circles are SPH collision simulation, over a range of parameters. We note that we do not see separate distinct processes at work here, but rather a single process o an energetic Erosive Hit-and-Run collision. We also predict the satellite-to-total mass ratio and primary density of objects that have not yet been observed to maintain a stable satellite system. These would be observations of Quaoar-like objects in density, with a much more massive moon.

As caveats we note that we assumed: zero-porosity densities; grazing collisions (H&R) included only if a remnant other than the target and projectile bodies exists (some erosion); minimum size of recorded remnant body is 100 SPH particles, to avoid spurious smoothing length issues.

Observable Remnant Systems

One main observable that can be influenced by collision history is the bulk density. Corresponding values for dwarf planets span a surprisingly large range (~1.5 – 3 g/cm^3), which is higher than mean densities of smaller TNOs [18, 19]. It has been suggested that the diversity of bulk densities, as well as the high occurrence of moons around dwarf planets, is the result of formation by at least several collision events between comparable mass bodies [18, 20]. Some material (preferentially ice) may be lost via fragmentation, as single-collision densification seems unlikely [18]. This leads to a hypothesized interpretation of densities of large icy bodies according to different collision regimes, pointing to a 2-mode process [20].

Figure 2 shows how the satellite-to-total mass ratio (designated as "q") relates the primary body's density. Our collision simulation results (in red) are superimposed over the measured data points (in black and gray) from the literature [20, 21]. We note that Orcus appears twice since estimates of its density differ, due to size uncertainty derived from albedo uncertainty [20]. Our results show how to reconstruct the distribution of observed systems, as a function of varying collision conditions. We note that nearly all collisions can be classified as Erosive Hit-and-Run.

This predicted collision regime, between disruption and partial merging, is characterized by large ejected mass, but small velocities relative to the mutual escape velocity of the system. Outcomes of this collision regime are sensitive to the specific collision parameters, but generally tend to be on the more energetic end – Higher velocities, smaller impact angles (< 45 deg) and/or smaller mass ratios.

Debris Cloud Distribution

Short-term evolution of material released through a collision is tracked self-consistently within the shock physics simulation. If the RMS velocity of the debris cloud is smaller than escape velocity of the residual target body in the post-collision system, then re-accretion will occur within a few orbital timescales [3].

Figure 3 shows the distributions of RMS velocities and associated masses of the debris clouds. These are post-simulation analyses of the SPH particles, which are not bound to any gravitational aggregate of 100 particles or more. We cut the analysis at 10 SPH particles, which may introduce mass (and acceleration) calculation errors, but these are on the order of ~20%. Mass and velocity are shown as a function of the accretion efficiency parameter, defined as (Mlr −Mt)/Mp [3]. This representation clearly identifies the different regimes and is easy to determine from collision calculations [3, 22].

The erosive H&R regime, distinguished by the vertical gray line, exhibits a larger scatter in the unbound mass, with more potential for mixed compositions, and a larger scatter in the RMS velocity field of each material cloud. Subsequently, debris material may have a higher probability of surviving on orbital timescales and escaping re-accretion onto the target body.

In order to get better estimates of how unbound fragments can survive the post-collision environment, we need to employ a more robust dynamical integration scheme. We follow the long-term evolution of unbound collision fragments with an N-body calculation scheme. We include all planets and additional gravitational potentials from the nearby surviving large remnant bodies (if they exist). Through these calculations we will be able to statistically determine plausible trajectories and re-accumulation paths of ejected material.

Figure 4 shows an example calculation for the orbital diffusion of collision ejecta around the primary's orbit. The example here is for a 150 km body at 15 AU. Fragments are approximated as 500 massless particles, initialized at random within an orbital element cube of size $da/a=de/e=di/i=10^{-5}$ (semi-major axis, *a*, eccentricity, *e*, and inclination, *i*). The other orbital angles were chosen randomly and the process was repeated 3 times, with random initial parameters and simulated run time of 10 Myr. This setup has fragments initially at up to 23,600 km from the central body (the presumed "largest remnant", after the collision event) and with very small deviations from its Keplerian velocity. Thus, the particles are near a minimally-bound initial orbit.

The orbits of the the fragments evolve due to the cumulative gravitational perturbations, but predominantly due to near-resonant interactions with Uranus. The separation (in AU) and dispersion (in km/s) evolve through time to cover a large range of $3x10^5$ km to 70 AU and 10^{-4} to 5 km/s, respectively. This is represented in the scatter of gray points. After ~50 Kyr the mean velocity dispersion is > 200 m/s, and the mean separation is > 0.5 AU. This means that a dynamical association between ejected fragments and the primary from which they came becomes very hard to identify. Thus, a scattrered collisional family would be much less probable to be associated with the primary beyond 50 Kyr from the ejection event. Interestingly, for some of the erosive H&R collisions (the more energetic ones) this dissociation of ejected fragments includes contributions from icy, hydrated and core-rock material. However, the mass and velocity distributions that determine the initial dynamical conditions are sufficiently distinct that there is effectively no component mixing in the debris clouds.

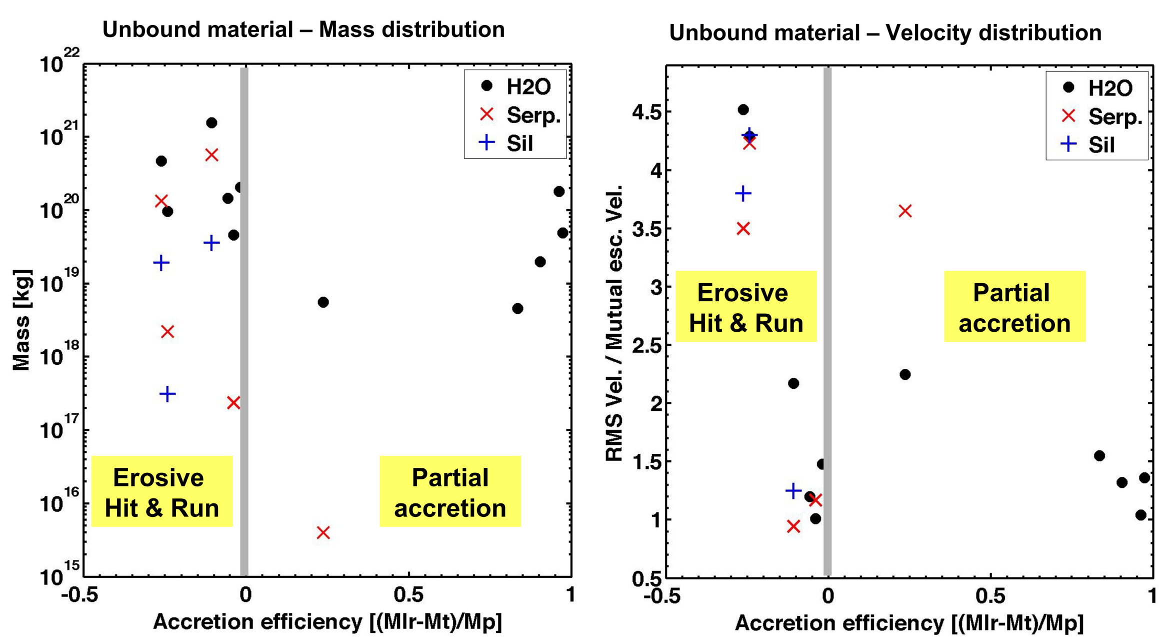

Figure 3: Debris mass distribution (left) and RMS velocities (right) as a function of the accretion efficiency parameter. Velocities are normalized to the mutual escape velocity of each collision system (target and projectile). Each data point is a collision simulation outcome considering total debris mass of specific material.

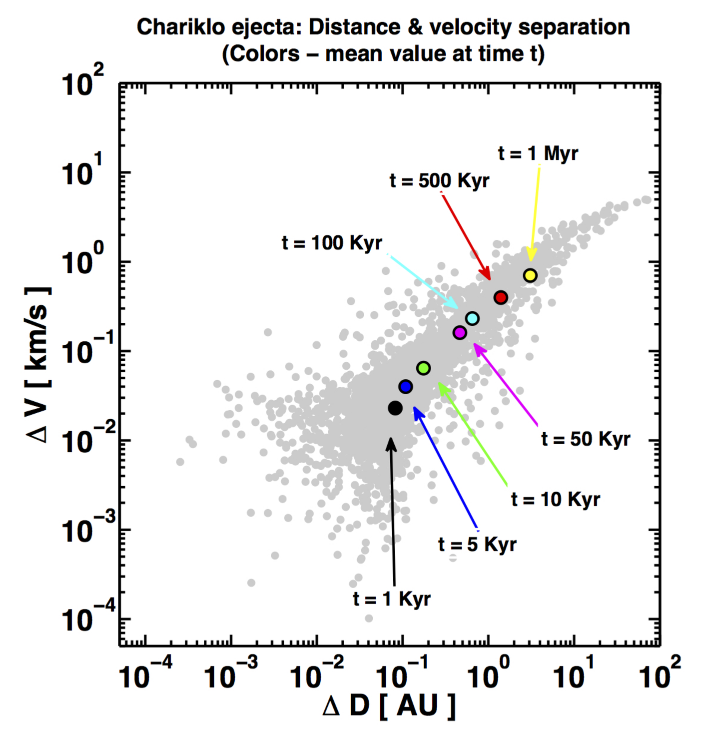

Figure 4: Dynamical evolution of fragments from a 150 km body at 15 AU, following gravitational perturbations with current solar system orbital conditions. Separation (relative distance, D, in AU) and dispersion (relative velocity, V, in km/s) are calculated for snapshots between 1Kyr-1Myr. Gray symbols show the distribution of all particles throughout the simulation. In color are the mean values for the fragment population at each recorded time (designated with a color arrow).

Conclusions

*** Erosive H&R collisions correspond to different satellite systems – Same process to densify, create variation in moon mass.**
*** Collisional debris can be mostly homogeneous and diverge quickly in the giant planet region.**

[1] Levison, H. F. et al. (2011) *AJ*, 142, 152. [2] Dones, L. et al. (2015) *SSRv*, 197, 191. [3] Asphaug, E. (2010) *Chemie der Erde*, 70, 199. [4] Asphaug, E. et al. (2015) *Asteroids IV*, U. of Arizona Press, 661.[5] Cuk, M. & Stewart, S. T. (2012) *Nature, 338*, 1047. [6] Canup, R. M. 2012, *Science*, 338, 1052. [7] Benz, W. et al. (2007) *SSRv.*, 132, 189. [8] Sarid, G. et al. (2014) *LPI Cont.*, 45, 2723. [9] Canup, R. (2011) *AJ, 141*, 35. [10] Leinhardt, Z. M. et al. (2010) *ApJ*, 714, 1789. [11] Sarid, G. & Stewart, S. T. (2013) *LPI Cont.*, 44, 1467. [12] Sarid, G. & Stewart, S. T. (2015) *LPI Cont.*, 46, 2834. [13] Springel, V. (2005) *MNRAS*, 364, 115. [14] Marcus, R. A. et al. (2009) *ApJL, 700*, L118. [15] Springel, V. & Hernquist, L. (2002) *MNRAS*, 333, 649. [16] O'Shea, B. W. et al. (2005) *ApJS*, 160, 1. [17] Sarid, G. et al. (2016) *IAU Proceedings*, 318, 9. [18] Brown, M. E. (2012), *AREPS*, 40, 467. [19] Grundy, W. M. et al. (2015) *Icarus*, 257, 130. [20] Barr, A. C. & Schwamb, M. E. (2016), *MNRAS*, 460, 1542. [21] Vilenius, E. et al. (2014) *A&A*, 564, 35. [22] Leinhardt, Z. M. & Stewart, S. T. (2012), *ApJ*, 745, 79 .